DOI: 10.1021/ma101279q

Macromolecules
ARTICLE

Interdiffusion in Polyelectrolyte Multilayers

Olaf Soltwedel,[†] Oxana Ivanova,[†] Peter Nestler,[†] Madlen Müller,[†] Ralf Köhler,[‡,§] and Christiane A. Helm*,[†]

[†]*Institut für Physik, Ernst-Moritz-Arndt Universität, Felix-Hausdorff-Str. 6, D-17487 Greifswald, Germany,* [‡]*Abteilung Grenzflächen, Max-Planck-Institut für Kolloid- und Grenzflächenforschung, Wissenschaftspark Potsdam-Golm, D-14424 Potsdam, Germany, and* [§]*Institut für Weiche Materie and funktionale Materialien, Helmholtz Zentrum Berlin für Materialien und Energie GmbH, Hahn-Meitner-Platz 1, 14109 Berlin, Germany*

Received June 9, 2010; Revised Manuscript Received July 19, 2010

ABSTRACT: Using neutron reflectivity, the internal structure of polyelectrolyte multilayers is described on the nanoscale. Each film consists of a protonated and a deuterated block, built from x protonated and y deuterated polycation/polyanion bilayers, respectively. The number of bilayers $N = x + y$ is kept constant; the position of the interface between the blocks is varied systematically. The polyanion is poly(styrenesulfonate) (PSS), and the polycation is poly(allylamine hydrochloride) (PAH) or poly(diallyldimethylammonium chloride) (PDADMAC). Always, the first four to five bilayers are thinner than the average bilayer thickness, but the three terminating bilayers are sometimes thicker. In the core zone, the bilayer thickness is constant. The internal roughness is smallest next to the film/air interface and increases with the number of bilayers away from the film/air interface. This suggests that each deposition step promotes the interdiffusion of the supporting layers. At the selected preparation conditions, the internal roughness increases more for PDADMAC/PSS than for PAH/PSS; the diffusion constants differ by 2 orders of magnitude.

Introduction

The ability to engineer surfaces that present multiple functionalities when and where they are needed could lead to important advances in electrooptical devices, separations, and biomaterials.[1−3] The layer-by-layer (LbL) assembly technique is ideally suited for such applications because it allows for absolute control over the sequence in which multiple functional elements are incorporated into a growing film.[4−6] However, the development of truly stratified, multicompartment LbL films with many biomacromolecules has been largely unsuccessful because of the phenomenon of interlayer diffusion, which results in blended structures lacking regular, controlled order on the nanometer scale.[5,7] To the best of our knowledge, the problem is not solved but only circumvented by up scaling: multicompartment films with micrometer-sized departments separated by barrier layers (thickness 50−100 nm) are described in the literature.[8,9] Therefore, it is desirable to quantify the internal structure (extension of single compartments, width of the internal interfaces) and the diffusion coefficient within the film on the nanoscale.[10,11]

All polyelectrolytes fall into one of two broad classes with respect to film growth: either the film thickness increases linearly with the number of deposition cycles[4] or exponentially.[7] Linearly growing films are thought to be stratified structures; the newly adsorbed layer diffuses into two or three top layers. Its density profile is broadened by the next two or three adsorbing layers, and then it is immobile.[4] Exponential growth is explained by high mobility of at least one polymer, which diffuses into the film, possibly until the substrate is reached.[7] Basically, exponential growth can be achieved in two ways: either by using polyelectrolytes which strongly bind water (i.e., many polypeptides and polysaccharides)[7] or by changing the deposition conditions of linearly growing films (i.e., most synthetic, strong polyelectrolytes) by adjusting salt concentration and/or temperature in the deposition solution.[12−14]

The standard system for linear film buildup is poly(allyl amine) (PAH) and poly(styrenesulfonate) (PSS).[4] In recent years, poly(diallyldimethyl ammonium chloride) (PDADMAC) is often used as polycation,[3,6,11,12] especially for biological applications. At room temperature, PDADMAC/PSS grows linearly. Yet, for certain preparation conditions PDADMAC/PSS grows exponentially.[12] This suggests a broad variety of diffusion constants within different films depending on preparation conditions, which goes beyond the two categories of PEMs (polyelectrolyte multilayers) outlined above.

To probe the thickness of each polycation/polyanion bilayer within the polyelectrolyte multilayer and to investigate layer interpenetration into neighboring layers, we use neutron reflection, which is sensitive to scattering length density (SLD) gradients along the surface normal. To quantify the internal roughness σ_{int}, we use a block architecture with x protonated and $N-x$ deuterated polyelectrolyte bilayers, as in $\mathrm{p}_x\mathrm{d}_{N-x}$ (cf. Figure 1).[15] This film architecture is advantageous since it allows to determine the roughness of the internal interface between the protonated and deuterated block unambiguously. Basically, the reflected neutron intensity is the sum of the interference patterns caused by three different layers: the total film (narrow oscillations) as well as the protonated and the deuterated parts of the film (both broader oscillations). In total, seven free parameters have to be fitted: both the protonated and the deuterated blocks have a scattering length density and thickness (4 parameters); the adjacent interfaces (the substrate/film, the inner, and the film/air interface) each have a roughness (3 additional parameters). Within confidence limits, the scattering length densities of the protonated and deuterated block can be determined independently from homogeneous films. Prior to the neutron reflectivity measurements, the roughness of the film/air and the substrate/film interface can be measured with X-ray reflectivity. With neutron reflectivity, the thickness of each

*To whom correspondence should be addressed.

 Published on Web 08/06/2010

block is obtained unambiguously from the width of the oscillations. Thus, the last remaining free parameter is the roughness of the internal interface between the blocks; it influences the decay of the interference patterns at large Q_z values and is determined from least-squares fits to the reflectivity data.

In the past, films with selectively deuterated polycation/polyanion bilayers were used to quantify the internal roughness.[4,15−19] The scattering length density profile of the thin deuterated layers resembles a Gaussian. In terms of unambiguous data fitting, this is a drawback: one can get almost the same Gaussian shape with a large height and a large width as with a small height and a small width. The height of the Gaussian corresponds to its scattering length density and its width to the roughness of the adjacent internal interfaces.[17] It is unfortunate that these important quantities cannot be determined independently. While important insights were achieved with the film architecture described above,[4,15−19] we think it is not ideally suited to investigate the internal structure of the film because of the parameter coupling.

Therefore, we choose the following approach: Each film consists of a protonated and a deuterated block, built from x protonated and $N - x$ deuterated bilayer pairs. The number of bilayers N is kept constant, and the position of the interface between the blocks is varied systematically. PAH/PSS and PDADMAC/PSS films are investigated. The preparation conditions are chosen to give a similar thickness for LbL films consisting of N polycation/PSS bilayers.

Materials and Methods

The polished surfaces of Si (100) wafers (Matthias Schmehl, Rostock, Germany) serve as negatively charged substrates. Branched polycation poly(ethylene imine) (PEI; M_w = 75 kDa; Aldrich, Germany) is an efficient first layer, and polycations PAH (M_w = 50−65 kDa; Aldrich Germany) or PDADMAC (M_w = 550 kDa; Polymer Standard Service, Mainz, Germany) are used for all subsequent layers. As polyanions, protonated PSS (M_w = 77.4 kDa) and deuterated PSSd (M_w = 83.7 kDa; both Polymer Standard Service, Mainz) are used. Ultrapure water is from Millipore (Milli-Q, Eschborn, Germany).

For the PAH/PSS films, all deposition solutions contain a polyelectrolyte concentration of 3 mmol/L (with respect to the monomer concentration) and 1 M NaCl (Merck, Darmstadt, Germany) at 40 °C. For the PDADMAC/PSS films, the polyelectrolyte concentration is 1 mmol/L and 0.1 M NaCl at 20 °C. The first PEI layer is always adsorbed at room temperature, yet the salt concentration is kept constant during PEM formation. Before use, the Si substrates are cleaned by using a standard RCA-1 procedure[15] and stored in pure water. The cleaned substrates are immersed in the respective polyelectrolyte solutions alternately (30 min for each adsorption step) and then washed three times in ultrapure water for 1 min each. PEMs are prepared by a robot (Riegler & Kirstein, Berlin, Germany). All solutions are kept at the same temperature, which is adjusted externally by a thermostat (Haake, ThermoFisher Scientific, Karlsruhe, Germany).

Reflectivity measurements are performed at nominal 0% RH (relative humidity). The film is placed into a gastight enclosure (THC, temperature−humidity chamber, Anton Paar GmbH, Graz, Austria) containing a Petri dish filled with P_2O_5 (Merck, Darmstadt, Germany). During alignment, the enclosure is flooded with dry nitrogen for 30 min. The relative humidity is constantly monitored with a humidity sensor (Hygrometer TH 309, B+B ThermoTechnik GmbH, Donaueschingen, Germany) and amounts to 0.5−2% RH. It varies slightly during the neutron experiments which take 6−7 h. To ensure that no change in the SLD or the thickness occurs during the measurement, each measurement is repeated at low Q_z (0.0028−0.033 Å^{-1}).

X-ray reflectometry experiments are performed with a Seifert XRD 3003 TT diffractometer (Seifert, Ahrensburg, Germany) using Cu Kα radiation (wavelength λ = 1.54 Å). The neutron measurements are carried out at instrument V6 at the neutron scattering facility of the Helmholtz Zentrum Berlin, Germany (λ = 4.66 Å).[20] In these reflectivity experiments, the deviation $\delta = 1 - n$ of the refraction index n from 1 depends linearly on material constants, which are directly related to the constituting molecules. For neutrons, the scattering length density SLD = $\sum n_i b_i / \sum n_i V_i$ is the relevant parameter, b_i is the scattering length, and V_i is the volume of atom i ($\delta = \lambda^2 \mathrm{SLD}/2\pi$). After the sums are performed, one finds that n only deviates by $\approx 10^{-5}$ from 1. Thus, approximations are possible, and the measured reflectivity R can be described as the Fresnel reflectivity R_F of an infinitely sharp interface modulated by interference effects from the thin surface layer.[21] Above a value of about two critical angles of total external reflection, the reflectivity is given by the kinematic approximation

$$\frac{R}{R_F} = \left| \frac{1}{\mathrm{SLD}_{Si}} \int \mathrm{SLD}'(z) e^{iQ_z z}\, dz \right|^2 \qquad (1)$$

Here, SLD_{Si} is the scattering length density of the bulk phase, $\mathrm{SLD}'(z)$ the gradient of the scattering length density along the surface normal, and Q_z the wave vector transfer normal to the surface.

The surface layer is parametrized as consisting of different slabs (each slab is described by a density and a thickness; each interface is characterized by a roughness parameter). Assuming two slabs in the sequence shown in Figure 1 (top), one obtains from eq 1

$$\begin{aligned} \frac{R}{R_F} = {} & A \exp(-Q_z{}^2 \sigma_{Si}{}^2) + B \exp(-Q_z{}^2 \sigma_{\mathrm{int}}{}^2) \\ & + C \exp(-Q_z{}^2 \sigma_{\mathrm{air}}{}^2) + D \exp\left(-\frac{Q_z{}^2}{2} (\sigma_{Si}{}^2 + \sigma_{\mathrm{int}}{}^2) \right) \cos(Q l_p) \\ & + E \exp\left(-\frac{Q_z{}^2}{2} (\sigma_{Si}{}^2 + \sigma_{\mathrm{air}}{}^2) \right) \cos(Q_z (l_p + l_d)) \\ & + F \exp\left(-\frac{Q_z{}^2}{2} (\sigma_{\mathrm{int}}{}^2 + \sigma_{\mathrm{air}}{}^2) \right) \cos(Q_z l_d) \end{aligned} \qquad (2)$$

with $A = ((\mathrm{SLD}_p - \mathrm{SLD}_{Si})/\mathrm{SLD}_{Si})^2$, $B = ((\mathrm{SLD}_d - \mathrm{SLD}_p)/\mathrm{SLD}_{Si})^2$, $C = (\mathrm{SLD}_d/\mathrm{SLD}_{Si})^2$, $D = (\mathrm{SLD}_p - \mathrm{SLD}_{Si})(\mathrm{SLD}_d - \mathrm{SLD}_p)/(\mathrm{SLD}_{Si})^2$, $E = (\mathrm{SLD}_p - \mathrm{SLD}_{Si})\mathrm{SLD}_d/(\mathrm{SLD}_{Si})^2$, and $F = (\mathrm{SLD}_d - \mathrm{SLD}_p)\mathrm{SLD}_d/(\mathrm{SLD}_{Si})^2$.

The parameter assignment is substrate (scattering length density SLD_{Si} and interfacial roughness σ_{Si}), protonated layer (scattering length density SLD_p, thickness l_p, and interfacial roughness σ_{int}), and deuterated layer (scattering length density SLD_d, thickness l_d, and film/air roughness σ_{air}). The first three summands are exponentially decaying offsets. Interesting are the last three summands. These cosine functions with exponentially decaying amplitudes are depicted in Figure 1 for a representative multilayer. The respective periodicities are determined by the thickness of the protonated block l_p, the film thickness $l_p + l_d$, and the thickness of the deuterated block l_d. How quickly each cosine function decays depends on the sharpness of the adjacent interfaces. Thus, σ_{Si} and σ_{int} determine the decay of the interference term with the thickness of the protonated block in the argument of the cosine function. Analogously, σ_{Si} and σ_{air} rule the term whose oscillations depend on the total film thickness $l_p + l_d$.

Always, the simulated reflectivity is convoluted with the angular divergence of the respective spectrometer (X-rays: 0.012°; neutrons: 0.017°). The exact matrix formalism is used to quantify the molecular parameters.[22]

Results

Figure 1 shows neutron reflectivity measurements of PEMs consisting of 14 polycation/polyanion bilayers. Both PAH/PSS

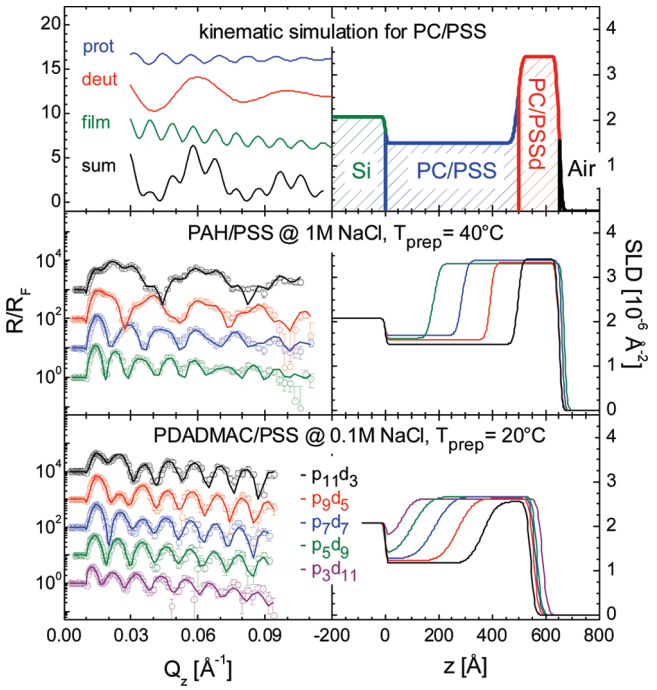

Figure 1. (top) Schematic of the scattering length density profile of a polyelectrolyte multilayer with block architecture (right) consisting of polycations (PC) and polyanions (PSS or deuterated PSSd). Also shown are the dominating contributions of the normalized neutron reflectivity, according to the kinematic approximation (cf. eq 2), i.e., the interference patterns caused by the protonated block (blue), the deuterated block (red), the total film (olive), and the sum of these contributions (black). (center and bottom) Left: normalized neutron reflectivity curves of p_xd_{14-x} polyelectrolyte multilayers, for PAH/PSS films (center) and PDADMAC/PSS films (bottom). The number of protonated and deuterated bilayers is indicated. The corresponding scattering length density profiles are shown on the right. The reflectivity curves are shifted vertically for clarity (left). Note that the simulated reflectivity curves are given on a linear scale (top), and the measurements are given on logarithmic scales (center and bottom).

and PDADMAC/PSS films are investigated; the preparation conditions are adjusted to achieve a similar film thickness (600−650 Å). The position of the internal interfaces is varied systematically using the following architectures: p_3d_{11}, p_5d_9, p_7d_7, p_9d_5, and $p_{11}d_3$ (p_3d_{11} not for PAH/PSS).

Considering the PAH/PSS films, the scattering length densities are such that the oscillation due to the deuterated block has the largest amplitude (cf. eq 2, the last term); therefore, it can be recognized in the reflectivity curves (cf. Figure 1). The $p_{11}d_3$ film has a thin deuterated block; therefore, the oscillation with a large amplitude and a large periodicity is superimposed by small periodicity beats attributed to the protonated block and the film. The p_9d_5 has a thicker deuterated part; therefore, a smaller periodicity of the dominating oscillation is observed. For the p_7d_7 and p_5d_9 films, the thickness of the deuterated block is increased further, leading to smaller periodicities.

For the PDADMAC/PSS films the scattering length density of the deuterated blocks is smaller than for the PAH/PSS films. This is due to the larger PDADMAC monomer volume (206 instead of 97 Å^3). Therefore, the contribution of the interference pattern of the deuterated block is less obvious. Furthermore, the large internal roughness causes pronounced damping for the interference patterns originating from the protonated and deuterated blocks. At high Q_z, only the interference pattern of the film survives (thickness $l_p + l_d$), and the neutron reflectivity curve is reminiscent of an X-ray reflectivity curve with its Kiessig fringes.

In the scattering length density profiles the shifting position of the interface between the two blocks can be clearly recognized. However, unexpected is the observation that the interface between the two blocks gets broader the further away it is located from the film/air surface. The effect is weak but unambiguous for the PAH/PSS films. For the PDADMAC/PSS film the internal roughness is already larger close to the film surface, and then it increases drastically. For the p_3d_{11} and the p_5d_9 films, the protonated block next to the substrate mixes so much with the deuterated block that the scattering length density of a pure protonated block is never reached. This suggests a blend of deuterated and protonated polyelectrolyte next to the substrate.

With the p_xd_{14-x} films (cf. Figure 1) it is found that the more bilayers separate an interface from the film/air surface, the larger is the interfacial width. To confirm this observation, films with different thickness and inverted architecture (d_xp_{N-x}) are investigated. For d_9p_7 and d_7p_7 the numbers of bilayers counted from the top of the film are the same, but the film thickness and the numbers of bilayers counted from the substrate are different. However, these films exhibit the same width of the internal interface (cf. Figure 2). The d_9p_5 film has the same thickness as the d_7p_7 film, yet its internal interface is closer to the film/air surface. The scattering length density profiles clearly show that the internal interface of the d_9p_5 film is more narrow than the d_7p_7 film; i.e., its internal roughness is smaller.

From the combination of the scattering length density profiles, the position of the internal interfaces within the films consisting of 14 bilayers is determined (cf. Figure 3). In the case of a constant bilayer thickness the internal interface would shift linearly with the number of deposited polyelectrolyte bilayers. However, the first few bilayers (4−5) within the films are thinner, an effect which is more pronounced for PDADMAC/PSS than for PAH/PSS. For PAH/PSS, the bilayer thickness is constant after the 4−5 precursor bilayers, even though a bit larger than the "average" bilayer thickness (calculated from the ratio of film thickness and bilayer number, $\langle d_{BL}\rangle = (l_p + l_d)/N = 4.6$ nm. For PDADMAC/PSS, the outer three bilayers next to film/air surface are thicker than the "average" bilayer thickness; in the film center the measured bilayer thickness corresponds to the average value.

The deviations are substantial. For PAH/PSS, the thickness of the precursor layer consisting of the first 4−5 polyelectrolyte bilayers is 70% of the value expected from linear growth (16 instead of 23 nm = $5\langle d_{BL}\rangle$). Because of the lack of a discernible outer layer, the majority of the PAH/PSS bilayers are 10% thicker than the average value (5.1 instead of 4.6 nm = $\langle d_{BL}\rangle$). For PDADMA/PSS, the thickness of the precursor layer is 47% of the expected value (10.8 instead of 23 nm). In the center layer the bilayer thickness corresponds to the average value. However, the thickness of the outer layer is 145% of the average value (20 instead of 13.8 nm = $3\langle d_{BL}\rangle$).

The combination of scattering length density profiles allows to quantify the relationship between the internal roughness and its position within the PEM (cf. Figure 3). It is shown as a function of bilayers away from the film/air surface (the "top of the PEM"), since we find that this parameter determines the roughness of the internal interface (cf. Figure 2). The data shown are those obtained not only from the scattering length density profiles depicted in Figure 1 but also from various other data (the sequence of protonated and deuterated block was exchanged; also the total number of bilayers was varied) shown in the Supporting Information. The square of the internal roughness σ_{int}^2 increases linearly with the distance from the film/air surface (note that also the film/air roughness is included). The effect is much more pronounced for PDADMAC/PSS (1.4 nm at the air/film surface increases to 5.4 nm at 7 bilayers below that surface) than for PAH/PSS (1.1 changes to 2.6 nm at 15 bilayers below).

For PDADMAC/PSS, the roughness does not increase further, when the interface positioned 9 or 11 bilayers below

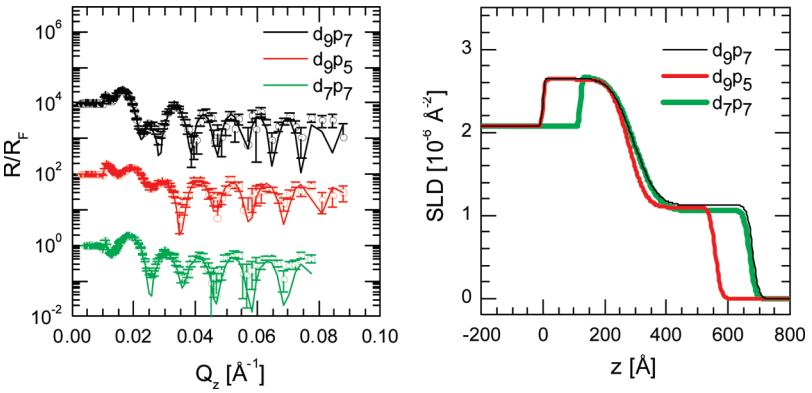

Figure 2. Normalized neutron reflectivity curves of PDADMAC/PSS film (d_9p_7, black) and corresponding scattering length density profiles. The same internal roughness is obtained, if the number of bilayers adjacent to the film/air surface is kept constant, even if there are less bilayers adjacent to the substrate (d_7p_7, green). However, if the number of bilayers next to the film/air surface is reduced, the internal interface is sharper (d_9p_5, red). Note that the d_9p_5 and the d_7p_7 films consist of the same number of bilayers and show the same thickness. The reflectivity curves are shifted vertically for clarity. For the scattering length density profiles, $z = 0$ corresponds to the substrate/film interface of the d_9p_7 and d_9p_5 films. The profile of d_7p_7 is shifted to higher z values to superimpose the internal interfaces.

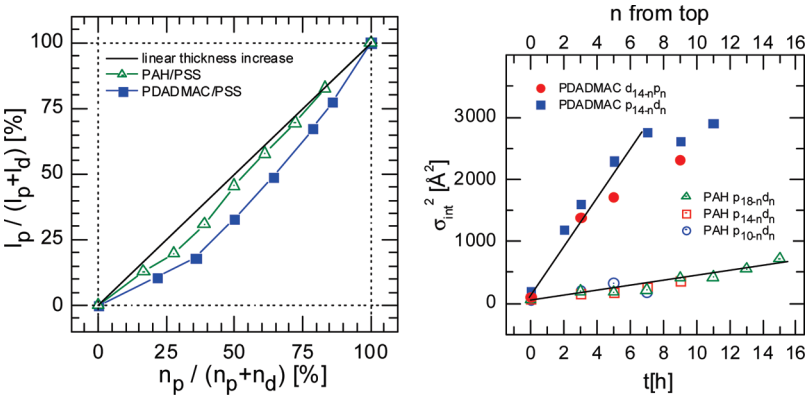

Figure 3. (left) Thickness of the protonated block l_p normalized by the total film thickness $l_p + l_d$ versus the number of bilayers in the protonated block n_p normalized by the total number of bilayers, $n_p + n_d$. The straight line is calculated assuming a constant polycation/polyanion bilayer thickness. (right) Square of the internal roughness ${\sigma_{int}}^2$ as a function of the number n of polyelectrolyte bilayers away from the film/air surface (top x-axis) or the time each interface was exposed to the deposition solution (bottom x-axis). Full symbols refer to PDADMAC/PSS and open symbols to PAH/PSS films. For each film the composition is indicated. The meaning of the symbols is the same on the left and the right side.

the film/air surface is considered (cf. p_9d_5 and $p_{11}d_3$ films in Figure 1). Note that the total number of bilayers is 14. Therefore, the interfaces with constant roughness are five or three bilayers away from the substrate. In that case, the scattering length density of the "protonated block" adjacent to the substrate is larger than expected for a pure protonated block (cf. Figure 1). Since this result violates mass conservation, presumably our simple model is not appropriate. The internal roughness at the last reliable measurement is very large (p_7d_7 film: $\sigma_{int} = 5.4$ nm). This high roughness is also indicated from the fast decay of the interference pattern caused by this internal interface (the relevant terms in eq 2 are $F\cdot\exp[(-{Q_z}^2/2)({\sigma_{int}}^2 + {\sigma_{air}}^2)]\cos(Q_z l_d)$ and $D\cdot\exp[(-{Q_z}^2/2)({\sigma_{Si}}^2 + {\sigma_{int}}^2)]\cos(Q_z l_p)$). Therefore, at this stage, we cannot resolve the internal interface for the p_9d_5 and $p_{11}d_3$ films reliably. On the basis of the data, it is not possible to decide if the increase of roughness continues or if it approaches a constant value.

The data can be explained by an ongoing mixing between the polycations and polyanions during each deposition step. To quantify our measurements in terms of diffusion, we assume two infinite reservoirs with the mixing time as the deposition time t.[23] Then, the concentration of deuterated PSS is given by

$$c_{PSSd}(z_0, t) = \frac{c_{PSSd,0}}{\sqrt{4\pi D t}} \int_{-\infty}^{z_0} \exp\left(-\frac{(z - l_p)^2}{4Dt}\right) dz \qquad (3)$$

l_p is the thickness of the protonated block, and D is the diffusion constant. The equation is very similar to the scattering length density profile obtained from eq 2

$$\mathrm{SLD}_d(z_0, t) = \frac{\mathrm{SLD}_d - \mathrm{SLD}_p}{\sigma_{int}\sqrt{2\pi}} \int_{-\infty}^{z_0} \exp\left(-\frac{(z - l_p)^2}{2\sigma_{int}^2}\right) dz \qquad (4)$$

Comparison of the arguments in the exponential function yields

$${\sigma_{int}}^2 = 2Dt \qquad (5)$$

Each measurement is a snapshot of the diffusion process, with the diffusion time determined by the position of the internal interface. Averaging over all positions, for PAH/PSS we obtain diffusion constant $D = 5.3 \times 10^{-20}$ cm^2 s^{-1} and for PDADMAC/PSS it is $D = 7.7 \times 10^{-18}$ cm^2 s^{-1}. Note that the diffusion constant in PDADMAC/PSS is 2 orders of magnitude larger.

However, a condition for the diffusion is the occurrence of an actual deposition step. The measured SLD profile of a PDADMAC/PSS film did not show any changes if measured a second time after 5 h of immersion in 1 M NaCl solution.

Discussion

We found that for linearly growing polyelectrolyte multilayers the internal roughness increases with the distance of the internal

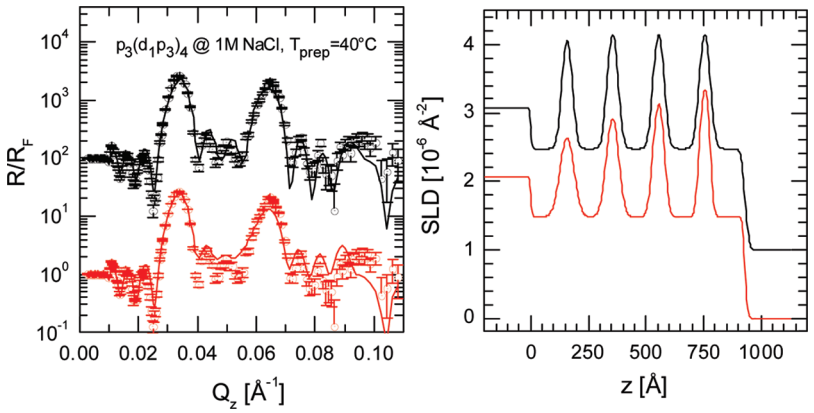

Figure 4. Normalized reflectivity curve of $(p_3d)_4p_3$ PAH/PSS films (1 M NaCl and 40 °C) from ref 17 with a fit assuming constant internal roughness (1.7 nm, black) and a simulation (red) assuming changing internal roughness depending on the position of the interface within the PEM. For the simulation, the roughness parameters are obtained from the block architecture PAH/PSS films with the same deposition conditions (cf. Figure 1). The corresponding SLD profiles are given as well (upper profile is shifted vertically by 10^{-6} Å^{-2}). (See Supporting Information for the resulting parameters of the fit and the simulation.)

interface from the film/air surface. In the literature, the internal roughness is deduced from films with selectively deuterated bilayers forming a superstructure, i.e., $(p_3d)_4p_3$. This film architecture leads to pronounced peaks in neutron reflectivity measurements.[4,16,17,24] In Figure 4, results from such a PAH/PSS film built from 1 M NaCl solution at 40 °C are shown. One fit is given with the standard model, a constant internal roughness.[4,16,17,22] Also, a simulation is shown, with the parameters as derived from the combined results of the PAH/PSS films with block architecture. The roughness increases with the separation from the film surface (scattering length density of the deuterated block as in Figure 1, the internal roughness increases as in Figure 2, parameter table in Supporting Information).

The simulation with increasing roughness away from the film−air interface looks very similar to the fit. Of course, by adjusting some parameters, the simulation would turn into a fit that describes the measured data better as the current simulation. Note that the scattering length density profiles obtained by the two different models are markedly different. The increased roughness close to the substrate leads to a diminished scattering length density of the adjacent deuterated bilayer. The reflectivity of a superstructure film alone does not give an unambiguous picture, but it is consistent with our results obtained with a series of films with the block architecture.

For the model assuming a constant internal roughness, $\langle\sigma_{int}\rangle$ = 1.65 nm = $0.36\langle d_{BL}\rangle$ was found to give the best fit, in agreement with the literature[25] ($\langle d_{BL}\rangle$ is the average bilayer thickness). For the model assuming variable roughness, the internal roughness is 1.2, 1.7, 2.2, or 2.6 nm, depending on its distance from the film/air interface (the values are obtained from fits to the measurements shown in Figure 1). If the internal roughness is compared to the average bilayer thickness $\langle d_{BL}\rangle$, one finds that it increases from $0.26\langle d_{BL}\rangle$ to $0.55\langle d_{BL}\rangle$. (These numbers are only true for the film consisting of 19 bilayers with $\langle d_{BL}\rangle$ = 4.95 nm, which exceeds $\langle d_{BL}\rangle$ = 4.6 nm for a film consisting of 14 bilayers; cf. Figure 1. Note that the average bilayer thickness $\langle d_{BL}\rangle$ increases with the number of bilayers, since the precursor layers are so thin; cf. Figure 2 and Supporting Information.) Concluding, the literature value[25] for the constant internal roughness of PAH/PSS films, $\langle\sigma_{int}\rangle \approx 0.4\langle d_{BL}\rangle$, is an approximation of the changing, position-dependent internal roughness.

Matters are more complicated for PDADMAC/PSS (prepared at 0.1 M and 20 °C). According to Figure 1, the internal roughness increases from 3.1 to 5.2 nm, i.e., from $0.75\langle d_{BL}\rangle$ to $1.25\langle d_{BL}\rangle$. No superstructure was found for the PDADMAC/PSS films at these conditions.[26] This is consistent with the internal roughness exceeding $\langle d_{BL}\rangle$ a few bilayers below the film/air interface. The only other published data concerning internal roughness for PDADMAC/PSS (at 0.1 M and 20 °C) are from ref 19 (and its Supporting Information) and amount to $0.33\langle d_{BL}\rangle$, but the PEMs were prepared by spin-coating and not by dipping as were ours and those described in ref 26. Presumably, spin-coating hinders interdiffusion of the layers and the internal interface is more narrow.

However, the diffusion coefficient found for these films is similar.[19] On immersion in high salt solutions, $D = 2.9 \times 10^{-17}$ cm^2 s^{-1} was found. This diffusion coefficient is a factor of 4 larger than our result. However, we found that diffusion only occurs during the deposition process, and we assumed that the diffusion occurs during the whole deposition time (30 min). If the deposition process is shorter than 30 min, then the diffusion coefficient is larger (cf. eq 5).

Even if the polyelectrolyte molecules adsorb as a stratified layer, during the following deposition cycles they interpenetrate into the layers above and below. The pronounced interpenetration leads to a more globular conformation which may be entropically more favorable than a stratified layer.

Roughness data are much larger for PDADMAC/PSS as for PAH/PSS. It is counterintuitive that interdiffusion occurs more easily if two strong polyelectrolytes are involved, as compared to one strong and one weak polyelectrolyte. PDADMAC has a larger degree of polymerization than PAH, but a shorter polymer should have the larger diffusion coefficient. A possible explanation could be that the laboratory conditions are close to the glass transition temperature of PDADMAC/PSS (ca. 35 °C), whereas a glass transition temperature of PAH/PSS was never found.[27]

Conclusion

Using neutron reflectivity, the internal structure of polyelectrolyte multilayers is described on a molecular scale. Polymer films are investigated which grow linearly with the number of deposition cycles. Each film consists of a protonated and a deuterated block, p_xd_{N-x} or d_xp_{N-x}. The number of polycation/polyanion bilayers N is kept constant; the position of the interface between the blocks is varied systematically. Different regions within the film are quantified-precursor zone, core zone, and outer zone can be distinguished. Always, the precursor zone (the first four to five bilayers) is thinner than the average bilayer thickness. For PDADMAC/PSS an outer zone can be identified (the three terminating bilayers); it is thicker. In the core zone, the bilayer thickness is constant and similar to the average bilayer thickness. One may conclude that the specific properties of the

respective zones depend on the polycation/polyanion pair used as well as on the preparation conditions.

Unexpected are the findings concerning the internal roughness. It is smallest next to the film/air interface and increases with the number of bilayers separating it from the film/air interface. Clearly, each deposition step promotes the interdiffusion of the supporting layers and thus increases the internal roughness. At the selected preparation conditions (PDADMAC/PSS at 20 °C and 0.1 M NaCl and PAH/PSS at 40 °C and 1 M NaCl), the diffusion constant of PDADMAC/PSS exceeds that of PAH/PSS films by 2 orders of magnitude. For PDADMAC/PSS we find next to the substrate blended layers.

Using the block architecture and neutron reflectivity, it is possible to identify polyelectrolyte multilayers with designated compartments and well-defined interfaces between adjacent layers on the nanoscale.

Acknowledgment. This work was supported by the BMBF (FKZ 03Z2CKI with the ZIK HIKE project), the DFG (He 1616/14-1), and the state of Mecklenburg-Vorpommern. M.M. and P.N. thank the University of Greifswald for support by undergraduate research programs.

Supporting Information Available: Figures S1−S3 and Tables S1−S6. This material is available free of charge via the Internet at http://pubs.acs.org.

References and Notes

(1) Hammond, P. T. *Adv. Mater.* **2004**, *16*, 1271–1293.
(2) Anderson, D. G.; Burdick, J. A.; Langer, R. *Science* **2004**, *305*, 1923–1924.
(3) Schlenoff, J. B. *Langmuir* **2009**, *25*, 14007–14010.
(4) Decher, G. *Science* **1997**, *277*, 1232–1237.
(5) Picart, C.; Mutterer, J.; Richert, L.; Luo, Y.; Prestwich, G. D.; Schaaf, P.; Voegel, J. C.; Lavalle, P. *Proc. Natl. Acad. Sci. U.S.A.* **2002**, *99*, 12531–12535.
(6) Schönhoff, M. *J. Phys.: Condens. Matter* **2003**, *15*, R1781–R1808.
(7) Ladam, G.; Schaad, P.; Voegel, J. C.; Schaaf, P.; Decher, G.; Cuisinier, F. *Langmuir* **2000**, *16*, 1249–1255.
(8) Garza, J. M.; Schaaf, P.; Müller, S.; Ball, V.; Stoltz, J. F.; Voegel, J. C.; Lavalle, P. *Langmuir* **2004**, *20*, 7298–7302.
(9) Mertz, D.; Vogt, C.; Hemmerle, J.; Mutterer, J.; Ball, V.; Voegel, J. C.; Schaaf, P.; Lavalle, P. *Nature Mater.* **2009**, *8*, 731–735.
(10) Skirtach, A. G.; Garageorgiev, P.; Bedard, M. F.; Sukhorukov, G. B.; Möhwald, H. *J. Am. Chem. Soc.* **2008**, *130*, 11572.
(11) Wood, K. C.; Chuang, H. F.; Batten, R. D.; Lynn, D. M.; Hammond, P. T. *Proc. Natl. Acad. Sci. U.S.A.* **2006**, *103*, 10207–10212.
(12) Büscher, K.; Ahrens, H.; Graf, K.; Helm, C. A. *Langmuir* **2002**, *18*, 3585–3591.
(13) Bouldmedais, F.; Ball, V.; Schwinte, P.; Frisch, B.; Schaaf, P.; Voegel, J. C. *Langmuir* **2003**, *19*, 440–445.
(14) Salomäki, M.; Vinokurov, I. A.; Kankare, J. *Langmuir* **2005**, *21*, 11232–11240.
(15) Ivanova, O.; Soltwedel, O.; Gopinadhan, M.; Köhler, R.; Steitz, R.; Helm, C. A. *Macromolecules* **2008**, *41*, 7179–7185.
(16) Gopinadhan, M.; Ahrens, H.; Günther, J. U.; Steitz, R.; Helm, C. A. *Macromolecules* **2005**, *38*, 5228–5235.
(17) Gopinadhan, M.; Ivanova, O.; Ahrens, H.; Günther, J. U.; Steitz, R.; Helm, C. A. *J. Phys. Chem. B* **2007**, *111*, 8426–8434.
(18) Tarabia, M.; Hong, H.; Davidov, D.; Kirstein, S.; Steitz, R.; Neumann, R.; Avny, Y. *J. Appl. Phys.* **1998**, *83*, 725–732.
(19) Jomaa, H. W.; Schlenoff, J. B. *Macromolecules* **2005**, *38*, 8473–8480.
(20) Mezei, F.; Golub, R.; Klose, F.; Toews, H. *Physica B* **1995**, *213*, 898–900.
(21) Baltes, H.; Schwendler, M.; Helm, C. A.; Heger, R.; Goedel, W. A. *Macromolecules* **1997**, *30*, 6633–6639.
(22) Parratt, L. G. *Phys. Rev.* **1954**, *95*, 359–369.
(23) Crank, J. *The Mathematics of Diffusion*; Oxford Science Publications: Oxford, 1989.
(24) Tarabia, M.; Hong, H.; Davidov, D.; Kirstein, S.; Steitz, R.; Neumann, R.; Avny, Y. *J. Appl. Phys.* **1998**, *83*, 725–732.
(25) Lösche, M.; Schmitt, J.; Decher, G.; Bowman, W. G.; Kjaer, K. *Macromolecules* **1998**, *31*, 8993.
(26) Steitz, R.; Klitzing, R. v. ILL, Experimental Reports **2003**, 9-11-894.
(27) Mueller, R.; Köhler, K.; Weinkammer, R.; Sukhorukov, G.; Fery, A. *Macromolecules* **2005**, *38*, 9766–9771.